


PAPER

[View Article Online](#)
[View Journal](#) | [View Issue](#)Cite this: *Nanoscale Adv.*, 2023, 5, 3267

Control and regulation of the performance of fullerene-based dye-sensitized solar cells with a D–D–A structure by external electric fields†

Xinyue Wang, Cong Shen, Jingping Li, Meixia Zhang* and Peng Song *

We investigated the modulating effect of an electric field (F_{ext}) on the photovoltaic properties of triphenylamine-based sensitizers with a D–D–A structure and compared the photovoltaic parameters at different electric field intensities. The results show that F_{ext} can effectively adjust the photoelectric properties of the molecule. From the change of the parameters that measures the degree of electron delocalization, it can be seen that the F_{ext} can effectively strengthen the electronic communication and promote the charge transfer process within the molecule. And the dye molecule under a strong F_{ext} has a narrower energy gap, more favorable injection, regeneration driving force and a larger conduction band energy level shift, which ensures that the dye molecule can exhibit larger V_{oc} and J_{sc} under a strong F_{ext} . The results of calculations on the photovoltaic parameters of dye molecules show that dye molecules can exhibit better photovoltaic performance under the action of F_{ext} , which provides beneficial predictions and prospects for the development of highly efficient DSSCs.

Received 23rd February 2023

Accepted 7th April 2023

DOI: 10.1039/d3na00115f

rsc.li/nanoscale-advances

1. Introduction

Dye-sensitized solar cells (DSSCs) are a promising photovoltaic technology due to their low raw material cost and high power conversion efficiency (PCE).¹ At present, the experimental power conversion efficiency has exceeded 13%,^{2–5} and the efficiency of small modules has exceeded 10%,⁶ but compared with traditional Si-based solar cells, its efficiency still needs to be developed. DSSCs are photovoltaic devices that graft photosensitizers and catalysts onto semiconductor electrodes to realize artificial photosynthetic systems.^{7,8} As an important component of DSSCs, redox-active photosensitizers play a key role in photo-generation of electrons, which affect the device performance by affecting the charge transfer process. In principle, they need to have suitable energy levels to ensure the injection of electrons, the efficient regeneration process of oxidation dyes, and a fast charge transfer process to reduce the occurrence of charge recombination processes.^{9,10} Currently, metal-based dyes, such as ruthenium (Ru) dye sensitizers, have high PCE efficiencies due to their broad light absorption range and better energy matching with TiO_2 .¹¹ However, their high cost, metal scarcity, and high-purity methods limit their large-scale application in DSSCs.^{12,13}

Compared with metal-based dyes, metal-free organic sensitizers have been developed as substitutes for metal-based dyes

because of their high molar extinction coefficient, low cost and easy purification.^{14–17} As a donor material, a triphenylamine sensitizer has high electron donating ability and good stability, which is a good choice for DSSCs.¹⁸ Intramolecular charge transfer is the most basic reaction in light energy conversion. The photoelectrons are injected from their molecular excited states into the conduction band of TiO_2 , but the molecules have a strong tendency to aggregate at the semiconductor surface, leading to the aggregation of molecules at the interface.^{19,20} The propeller-like molecular structure of TPA can not only effectively alleviate the aggregation of molecules at the interface and promote the electron injection process at the interface, but also effectively inhibit the recombination of redox couples (I^-/I_3^-).²¹ Furthermore, boron dipyrromethene (BODIPY), as a popular sensitizer, possesses a flexible geometry that can easily change its spectral and photophysical properties through minor modifications to its structure.^{22–24} The characteristics and photovoltaic characteristics of organic sensitizers are directly related to the molecular structure, and the photovoltaic characteristics of the molecules can be improved by structural modification, which in turn can improve the PCE. Sharma *et al.* formed a triplet $\text{PorCOOH}-(\text{BDP})_2$ by covalently bonding two BODIPY groups with 1,3,5-triazine. The introduction of BODIPY not only enhances the light absorption of the dye at 500 nm, but also promotes the electron injection process and improves the energy level alignment of dye regeneration.²⁵

To this end, building on the work of Benitz *et al.*, we investigated a TPA-based dual-donor dye molecule TPA-TT-BODIPY- C_{60} (Fig. 1), in which triphenylamine (TPA)-tertithiophene (TT) is the first donor and BODIPY is the second donor.²⁶ So far,

College of Physics, Liaoning University, Shenyang 110036, China. E-mail: ldzmx@sina.com; songpeng@lnu.edu.cn; Tel: +86-24-62202306

† Electronic supplementary information (ESI) available. See DOI: <https://doi.org/10.1039/d3na00115f>

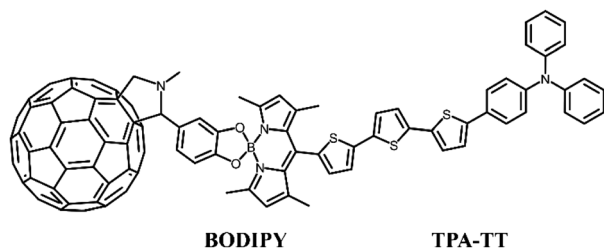


Fig. 1 Structural formula of TPA-TT-BODIPY-C₆₀.

fullerenes and their derivatives have become promising materials for DSSCs, and the insertion of BODIPY provides a bridge between TPA-TT and fullerenes for efficient charge transfer, which is a good charge transfer promoter.^{27,28} The formed dual-donor structure can break the light absorption limitation of the D-A system and increase the charge transfer path, thus improving the efficiency of the cell device. In addition, experiments show that TPA-TT-BODIPY-C₆₀ exhibits photoinduced charge separation in polar benzonitrile and non-polar toluene, and the long-lived charge separation state of TPA-TT-BODIPY-C₆₀ is about 20 ns due to the hole displacement mechanism. Considering that the external electric fields (F_{ext}) are usually able to modulate the charge transfer process, an effective intramolecular charge transfer process is a key factor in improving the photovoltaic performance of dyes.^{29–31} Moreover, so far, there are few reports on the application of F_{ext} to DSSC devices, and the photophysical research of DSSCs under the action of F_{ext} is still lacking. In this context, in order to find effective strategies to improve device performance, the effect of F_{ext} variation on the photovoltaic parameters affecting the device was investigated.

In this study, the electronic structures and light absorption properties of dye molecules at different F_{ext} intensities were calculated by using DFT and TDDFT. The aim was to investigate the effect of F_{ext} on key parameters that have a direct effect on dye short-circuit current density (J_{sc}) and photovoltage (V_{oc}), which include light harvesting efficiency (LHE), electron injection driving force (ΔG_{inject}), driving force of regeneration (ΔG_{reg}), conduction band shift (ΔE_{CB}), etc. It is shown by calculations that the addition of F_{ext} can indeed modulate the photoelectric properties of the TPA-TT-BODIPY molecule. And the increase of electric field strength makes the dye molecules have better ΔG_{inject} , ΔG_{reg} and larger ΔE_{CB} , which further enhances the photocurrent and voltage. Therefore, we hope to provide theoretical guidance for further optimization of DSSCs by elaborating the research results of the optoelectronic properties of the dye molecule under the action of the F_{ext} .

2. Calculation details

All calculations in this work were performed using the density functional theory (DFT) and time-dependent DFT (TD-DFT) of the Gaussian 09 software.^{32–34} The ground-state structures before and after the dye was bound to $\text{Ti}(\text{OH})_3 \cdot \text{H}_2\text{O}$ were optimized by DFT using the B3LYP functional and 6-31G(d) basis set, where the Ti atom was based on the LANL2DZ basis set.^{35–39}

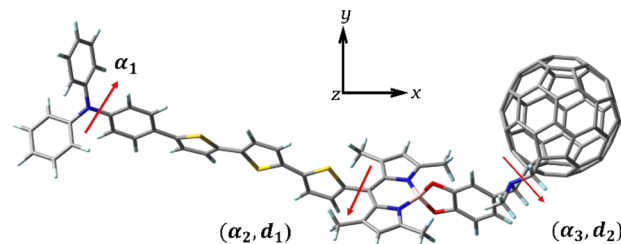


Fig. 2 Three-dimensional structure of TPA-TT-BODIPY-C₆₀. The F_{ext} is in the direction of the x coordinate.

Considering the long-range interaction, the excited-state transition properties before and after dye binding to $\text{Ti}(\text{OH})_3 \cdot \text{H}_2\text{O}$ were calculated using the long-range Coulomb decay CAM-B3LYP functional under TD-DFT theory, and the absorption spectra of the dye were simulated by Multiwfn software.^{40–42} For studying the effect of solvent on charge transfer, the solvent effect of benzonitrile solvent was simulated in calculations using a polarizable continuous medium model (IEF-PCM) in the form of integral equations.^{43,44} At the B3LYP/6-31G(d) level, single-point energy calculations were performed on the geometries of the cationic and anionic states of the optimized dye to obtain the total reorganization energy (λ_{total}) of the dye. Using a finite field approach, the F_{ext} is set in the direction of the x-coordinate (Fig. 2), with the strength between -10×10^{-5} – 10×10^{-5} a.u., and the effect of the F_{ext} on the parameters affecting the photovoltaic characteristics of the cell is investigated.

3. Results and discussion

3.1. Molecular structure

It is well known that the charge transfer efficiency of dye molecules is closely related to the molecular structure, and efficient intramolecular charge transfer is a key factor affecting DSSCs. The PCE of DSSCs decreases due to the aggregation of dye molecules, so the aggregation phenomenon of molecules can be improved by changing the structure of molecules appropriately. On the one hand, by improving the molecular aggregation caused by planar molecules, and on the other hand, by the modulating effect of the electric field on improving the charge transfer efficiency, the non-planar dye molecule (TPA-TT-BODIPY) with a double donor structure at different F_{ext} strengths is studied in this paper.

The respective dihedral angles and bond lengths of the studied dye at different F_{ext} strengths are shown in Table 1. α_1 is the dihedral angle of the donor (TPA) itself, and α_2 and α_3 are the dihedral angles between BODIPY and thiophene and the acceptor, respectively (Fig. 2). The α_1 is in the range of 43–45°, indicating that the TPA exhibits a distorted conformation to some extent, and the distorted donor structure weakens the accumulation of the dye molecule on the semiconductor surface and improves the electron injection process. The dihedral angles α_2 and α_3 are in the range of 87° and 98°, respectively, indicating the formation of a torsional structure between BODIPY and thiophene/acceptor, which can effectively improve the π - π aggregation between dye molecules and ensure the



Table 1 Dihedral angles($^{\circ}$) and bond lengths(\AA) of TPA-TT-BODIPY in F_{ext} (F_{ext} in 10^{-5} a.u.)

| F_{ext} | α_1 | α_2 | α_3 | d_1 | d_2 |
|------------------|------------|------------|------------|---------|---------|
| -10 | 43.838 | 87.412 | 98.064 | 1.48345 | 1.51346 |
| -7 | 43.965 | 87.404 | 98.082 | 1.48342 | 1.51344 |
| -5 | 44.054 | 87.383 | 98.078 | 1.48342 | 1.51343 |
| -3 | 44.151 | 92.376 | 98.084 | 1.48342 | 1.51342 |
| -1 | 43.840 | 92.376 | 98.476 | 1.48344 | 1.5131 |
| 0 | 44.266 | 87.369 | 98.098 | 1.4834 | 1.5134 |
| 1 | 44.295 | 87.357 | 98.089 | 1.48338 | 1.5134 |
| 3 | 44.396 | 87.336 | 98.094 | 1.48337 | 1.51339 |
| 5 | 44.481 | 87.322 | 98.097 | 1.48336 | 1.51338 |
| 7 | 44.578 | 87.351 | 98.102 | 1.48336 | 1.51337 |
| 10 | 44.715 | 87.164 | 98.107 | 1.48332 | 1.51336 |

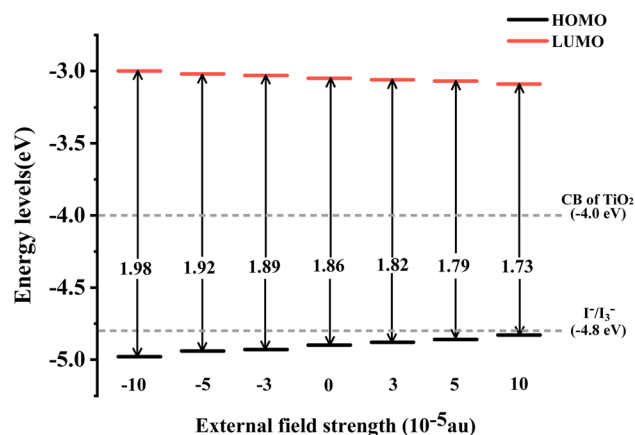
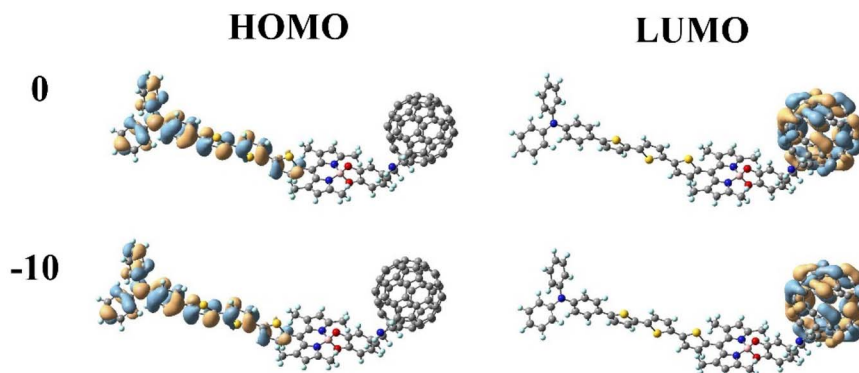
improvement of their thermal stability. The bond length d_1 between thiophene and BODIPY is about 1.4833 to 1.4835 \AA , which is close to the bond length of C=C, which is beneficial for the intramolecular charge transfer. The bond length d_2 between BODIPY and the acceptor is in the range of 1.5134–1.5135 \AA and gradually shortens with increasing F_{ext} strength, which will facilitate efficient ICT from the BODIPY to the acceptor. In fact, the addition of the F_{ext} had no appreciable effect on these parameters and did not change the molecular structure to a large extent. In fact, the addition of F_{ext} has no obvious effect on these parameters, so it can be seen that F_{ext} does not have a great effect on the molecular structure.

3.2. Electronic structure

In DSSCs, the efficient charge-separated states are closely related to the electronic excitation of the frontier molecular orbitals. To gain insight into the correlation between electronic properties and the molecular structure at different F_{ext} intensities, we mapped the electron density of frontier molecular orbitals (FMOs) of dye molecules at different F_{ext} intensities. As shown in Fig. 3, the highest occupied molecular orbital (HOMO) is distributed on the donor TPA-TT and the lowest unoccupied molecular orbital (LUMO) is distributed on the acceptor C_{60} . This distribution can effectively separate the charges, making the long-distance charge transfer process easier to occur. The

HOMO to LUMO transition can result in charge transfer from TPA-TT to C_{60} , resulting in electron injection. Under the effect of the F_{ext} , the electron densities of FMOs of dye molecules are less affected by the F_{ext} and show similar distribution characteristics.

The energy level of the dye molecule is a key factor affecting electron injection and dye regeneration. As shown in Fig. 4, under different F_{ext} conditions, the LUMOs of the dye located above the conduction band of TiO_2 (-4.0 eV) indicate that the excited dye has efficient charge injection capability. The HOMOs of the dye are lower than the redox potential of the electrolyte (I^-/I_3^-), which ensures that the dye that loses electrons can gain electrons from the electrolyte, thereby realizing the dye regeneration process. At $F_{\text{ext}} = 10 \times 10^{-5}$ a.u., the energy level of the HOMO is -3.09 eV, which is 0.09 eV lower compared to -3.00 eV at $F_{\text{ext}} = -10 \times 10^{-5}$ a.u., as shown in the schematic energy diagram in Fig. 4. We found that when the F_{ext} strength changes, the LUMO energy level is relatively stable, but the HOMO–LUMO energy gap (E_g) becomes smaller and smaller. Therefore, it can be seen that the change mainly comes from the effect of the F_{ext} on the stability of the HOMO. The reduced energy gap makes the molecule more easily excited, improves the light absorption capacity of the molecule in the long wavelength region, and further improves the power conversion

**Fig. 4** Schematic energy diagram of TPA-TT-BODIPY in F_{ext} .**Fig. 3** Frontier molecular orbitals (FMOs) of TPA-TT-BODIPY in F_{ext} (F_{ext} in 10^{-5} a.u.).

efficiency. The charge transfer reaction is the most fundamental reaction in light energy conversion and is an important factor affecting the conversion efficiency. In our previous work, it was found that in the TPA-TT-BODIPY-C₆₀ molecule, charge transfer occurred not only between C₆₀ and the two electron donors, but also between the two electron donors due to the difference in electron donating ability. This opens up more possibilities for multiple charge transfer pathways.

3.3. Nonlinear optical properties

Dye molecules are receiving increasing attention for their good nonlinear optical (NLO) response for a wide range of applications in data storage, sensors, *etc.* The impact is that electronic properties of the molecule are the key factors affecting the NLO properties, and materials with low energy gaps and efficient charge transfer efficiency exhibit good NLO properties. The change in hyperpolarizability (β) is an indicator of nonlinear optical properties and is a key parameter to measure the degree of electron delocalization. We investigated the correlation between the electric field, NLO properties and molecular structure by calculating the hyperpolarizability of the dye at different electric field strengths. According to the FF method combined with the electronic structure method the first hyperpolarizability (β_{tot}) is expressed as:^{45,46}

$$\beta_{\text{tot}} = \sqrt{\beta_x^2 + \beta_y^2 + \beta_z^2} \quad (1)$$

where β_x , β_y and β_z are the components of the second-order polarizability tensor along the x , y , and z directions, respectively, and the first hyperpolarizability is a third-order tensor that can be further represented by the component matrix traces:

$$\beta_x = \beta_{xxx} + \beta_{xyy} + \beta_{xzz} \quad (2)$$

$$\beta_y = \beta_{yyy} + \beta_{xxy} + \beta_{zyy} \quad (3)$$

$$\beta_z = \beta_{zzz} + \beta_{xxz} + \beta_{yyz} \quad (4)$$

The calculated first hyperpolarizabilities of the dye molecules and their x , y , and z components are shown in Table 2. The β_{tot} of the dye is 4297 a.u. in the absence of F_{ext} . Compared with β_{tot} in $F_{\text{ext}} = 0$, the hyperpolarizability of the dye at all F_{ext} intensities is improved, indicating that the addition of F_{ext} can

indeed increase the β value of dye molecules. In the case of increasing F_{ext} strength, β_{tot} exhibits a gradually increasing trend, which is consistent with the change in the energy gap. A decrease in the energy gap makes the electron excitation easier, and the hyperpolarizability increases. The β values of the three components were compared, and it was found that the β value in the x direction was significantly larger than the β value in the y/z direction, indicating that the first hyperpolarizability was mainly contributed by the x -direction, indicating that the charge transfer was mainly along the x -direction. Moreover, under the external electric conditions, $|\beta_{xxx}|$ at $F_{\text{ext}} = 10 \times 10^{-5}$ a.u. produces an increment of 524 relative to $|\beta_{xxx}| = 3435$ at $F_{\text{ext}} = -10 \times 10^{-5}$ a.u. This indicates that the increase mainly originates from the charge transfer direction (X direction), which also proves that the β_{tot} can promote electron excitation and thus modulate the NLO properties. For asymmetric systems the dipole moment is the most commonly used physical indicator to determine the polarity of a molecule, which essentially reflects the separation of the positive and negative charge centers of the system. We found that the dipole moment increases with increasing electric field by calculating the dipole moment under different electric fields (Table S1[†]), which further supports the results obtained from the β_{tot} .

3.4. Dye adsorption on TiO₂

We further evaluated the light-absorbing ability of the dye molecules by calculating the UV-vis absorption spectra of the dye molecule. Fig. 5 shows the absorption spectra of the dye obtained by Gaussian broadening (broadening parameter of 0.3 eV). The spectrum is mainly composed of two absorption bands, with the main absorption band appearing at 394–453 nm, as shown in Fig. 5. The excitation parameters of the excited states corresponding to the strongest absorption peaks at different F_{ext} intensities are shown in Table 3. However, at different F_{ext} intensities, its absorption spectrum does not change much, which can be seen from the change of its maximum absorption wavelength. Under the condition of $F_{\text{ext}} = 0$, the strongest absorption peak is mainly contributed by the excited states of S_8 , S_{12} and S_{15} , and the corresponding maximum absorption wavelength is 420 nm. The corresponding oscillator strengths are 0.3707, 1.5667 and 0.5095, indicating that the strongest absorption peak is mainly contributed by S_{12} , and the excited

Table 2 Hyperpolarizability (a.u.) of the dye in F_{ext} (F_{ext} in 10^{-5} a.u.)

| F_{ext} | β_{xxx} | β_{xyy} | β_{xzz} | β_{yyy} | β_{xxy} | β_{zyy} | β_{zzz} | β_{xxz} | β_{yyz} | β_{xyz} | β_{tot} |
|------------------|---------------|---------------|---------------|---------------|---------------|---------------|---------------|---------------|---------------|---------------|----------------------|
| −10 | −3435 | −549 | −350 | −226 | −144 | −132 | 40 | 123 | 94 | −182 | 4363 |
| −7 | −3514 | −551 | −351 | −225 | −143 | −132 | 40 | 124 | −225 | −183 | 4455 |
| −5 | −3566 | −552 | −352 | −225 | −142 | −132 | 40 | 125 | 95 | −183 | 4498 |
| −3 | −3619 | −553 | −352 | −225 | −141 | −132 | 40 | 126 | 95 | −183 | 4552 |
| −1 | −3661 | −562 | −341 | −254 | −196 | −127 | 16 | 138 | 70 | −145 | 4601 |
| 0 | −3404 | −552 | −308 | −255 | −146 | −127 | 111 | 36 | 91 | −214 | 4297 |
| 1 | −3721 | −556 | −354 | −225 | −140 | −132 | 41 | 128 | 95 | −184 | 4657 |
| 3 | −3774 | −557 | −354 | −224 | −139 | −132 | 41 | 128 | 95 | −184 | 4712 |
| 5 | −3826 | −558 | −355 | −224 | −138 | −132 | 41 | 129 | 95 | −185 | 4765 |
| 7 | −3879 | −560 | −356 | −224 | −138 | −132 | −356 | 130 | 96 | −185 | 4836 |
| 10 | −3959 | −560 | −357 | −224 | −137 | −131 | 42 | 130 | 96 | −186 | 4902 |



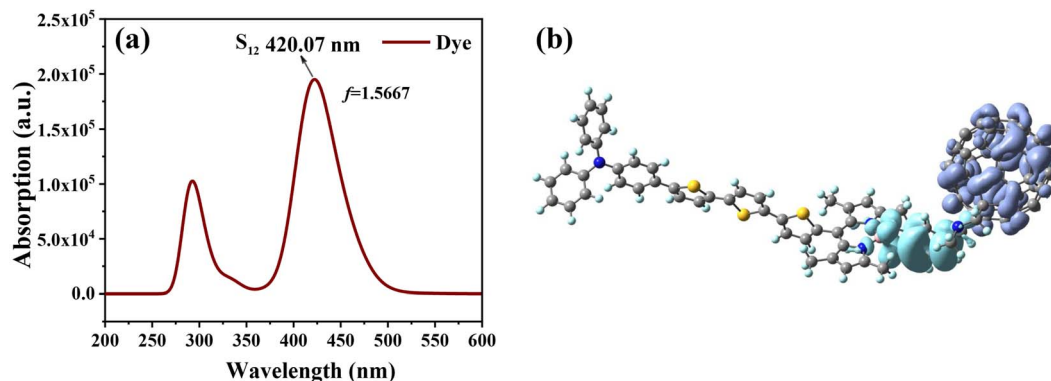


Fig. 5 Simulated UV-vis absorption spectrum of the dye molecule (a) and charge density difference (CDD) of S_{12} (b); in CDD, purple represents electrons and blue represents holes.

Table 3 Electronic transition energy (ΔE), maximum absorption wavelength (λ_{max}), oscillator strength (f) and main configuration of the dye molecule in F_{ext} (F_{ext} in 10^{-5} a.u.)^a

| F_{ext} | State | $\Delta E/\text{eV}$ | $\lambda_{\text{max}}/\text{nm}$ | f | Main configuration |
|------------------|-------|----------------------|----------------------------------|--------|--------------------|
| −10 | 12 | 2.9652 | 418.12 | 1.7877 | 61.56% (H–L+4) |
| −7 | 12 | 2.9613 | 418.68 | 1.7405 | 59.15% (H–L+4) |
| −5 | 12 | 2.9587 | 419.0 | 1.6976 | 59.15% (H–L+4) |
| −3 | 12 | 2.9559 | 419.45 | 1.6512 | 55.04% (H–L+4) |
| 0 | 12 | 2.9515 | 420.07 | 1.5667 | 51.39% (H–L+4) |
| 3 | 12 | 2.9460 | 420.85 | 1.4700 | 47.37% (H–L+4) |
| 5 | 12 | 2.9423 | 421.38 | 1.3961 | 44.44% (H–L+4) |
| 7 | 12 | 2.9390 | 421.87 | 1.3123 | 41.35% (H–L+5) |
| 10 | 11 | 2.9303 | 423.11 | 1.2125 | 36.77% (H–L+5) |

^a In CI, H is the HOMO and L is the LUMO.

state parameters of the other excited state are shown in Table S2.† For S_{12} , it can be seen from its charge density difference (CDD) (Fig. 5b) that electrons and holes are distributed on fullerenes and BODIPY, respectively, which can identify S_{12} as intramolecular charge transfer excitation from BODIPY to fullerene. When the F_{ext} strength increases, the absorption peak appears slightly red-shifted, and the maximum absorption wavelength and oscillator strength also change accordingly.

The DFT theory was used to simulate the adsorption structure of the dye and TiO_2 (Fig. 6), and to study the interaction between the dye and semiconductor surfaces. The dye molecule is connected by a carboxylic acid group and TiO_2 via a bidentate bridging, and has been shown to be the most stable chemisorption model.^{47,48} We considered different F_{ext} strengths to study the effect of F_{ext} on the energy gap. The carboxylic acid-linked bidentate bridge enables the adsorption of molecules on the $\text{Ti}(\text{OH})_3 \cdot \text{H}_2\text{O}$ surface, and the stability of this bidentate bridge adsorption mode makes it the preferred adsorption mode. To gain more insight into the electronic coupling between the dye and the TiO_2 conduction band, we calculated the electronic structure of the dye- TiO_2 system, and the energy levels of the FMOs are shown in Table 4.

As shown in Table 4, under the condition of $F_{\text{ext}} = 0$, the HOMO of the dye- TiO_2 did not change compared to that of a single dye, while the LUMO level decreased significantly, resulting in a smaller energy gap. The decrease of the LUMO level indicates that the dye and the TiO_2 conduction band have strong electronic coupling, which is favorable for the electron injection process. In fact, the changes in the HOMO and LUMO under the F_{ext} are opposite to those of a single dye, which leads to a somewhat larger energy gap with increasing F_{ext} . In the range of $F_{\text{ext}} = -10$ to 3×10^{-5} a.u., the energy gap of dye- TiO_2

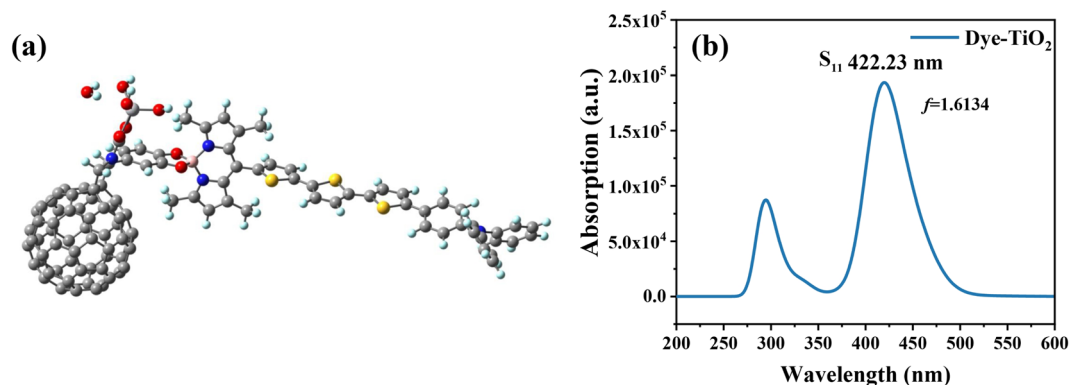


Fig. 6 Three-dimensional structure of dye- TiO_2 (a), and simulated UV-vis absorption spectrum of dye- TiO_2 (b).



Table 4 LUMO level, HOMO level and energy gap of the dye and dye-TiO₂ in F_{ext} (F_{ext} in 10^{-5} a.u.)

| F_{ext} | Dye | | | Dye-TiO ₂ | | |
|------------------|-------|-------|-------|----------------------|-------|-------|
| | LUMO | HOMO | E_g | LUMO | HOMO | E_g |
| −10 | −3.00 | −4.98 | 1.98 | −3.14 | −4.82 | 1.67 |
| −7 | −3.02 | −4.96 | 1.94 | −3.13 | −4.84 | 1.71 |
| −5 | −3.02 | −4.94 | 1.92 | −3.12 | −4.86 | 1.73 |
| −3 | −3.03 | −4.93 | 1.89 | −3.11 | −4.87 | 1.76 |
| −1 | −3.04 | −4.91 | 1.87 | −3.11 | −4.89 | 1.78 |
| 0 | −3.05 | −4.90 | 1.86 | −3.10 | −4.90 | 1.79 |
| 1 | −3.05 | −4.90 | 1.84 | −3.11 | −4.90 | 1.80 |
| 3 | −3.06 | −4.88 | 1.82 | −3.10 | −4.92 | 1.82 |
| 5 | −3.07 | −4.86 | 1.79 | −3.09 | −4.93 | 1.84 |
| 7 | −3.08 | −4.85 | 1.77 | −3.08 | −4.95 | 1.87 |
| 10 | −3.09 | −4.83 | 1.73 | −3.07 | −4.97 | 1.90 |

is lower than that of a single dye, indicating that negative and weak electric fields are more favorable for electron injection.

The combination of the dye with Ti(OH)₃·H₂O causes a change in the optical properties of the dye. Therefore, using the TD-DFT method, the UV-vis absorption spectrum of dye-TiO₂ was calculated, and the corresponding excited state parameters are shown in Table 5. The absorption spectra of the dye-TiO₂ are not very different from those of a single dye, and their main absorption bands are mainly distributed in the range of 410–453 nm, as shown in Fig. 6. When there is no electric field, the maximum absorption wavelength of dye-TiO₂ has a slight blue shift, and the oscillator strength is also improved. Unlike the dye alone, the maximum absorption wavelength of the dye-TiO₂ system under a negative F_{ext} corresponds to S₁₁. Under the action of a positive F_{ext} , the corresponding oscillator strength also increases, and with the increase of the F_{ext} , its maximum absorption wavelength also gradually exhibits a blue shift, which is opposite to the case of a single dye. The main orbital contribution of dye-TiO₂ corresponding to λ_{max} shows that the orbital contribution of dye-TiO₂ is slightly different from that of the separated dye as well. This may be due to the appearance of new excitons in the interaction of the dye with TiO₂.

Table 5 Electronic transition energy (eV), maximum absorption wavelength (λ_{max}), oscillator strength (f), and main configuration of dye-TiO₂ in F_{ext} (F_{ext} in 10^{-5} a.u.)^a

| F_{ext} | State | $\Delta E/\text{eV}$ | $\lambda_{\text{max}}/\text{nm}$ | f | Main configuration |
|------------------|-------|----------------------|----------------------------------|--------|--------------------|
| −10 | 11 | 2.9167 | 425.08 | 1.3001 | 40.63% (H-L+5) |
| −7 | 11 | 2.9235 | 424.1 | 1.4037 | 44.77% (H-L+5) |
| −5 | 11 | 2.9273 | 423.54 | 1.4698 | 47.45% (H-L+5) |
| −3 | 11 | 2.9313 | 422.97 | 1.5309 | 50.01% (H-L+5) |
| 0 | 11 | 2.9364 | 422.23 | 1.6134 | 53.53% (H-L+4) |
| 3 | 12 | 2.9604 | 420.85 | 2.0115 | 73.44% (H-L+4) |
| 5 | 12 | 2.9621 | 418.57 | 2.0263 | 74.29% (H-L+4) |
| 7 | 12 | 2.9648 | 418.19 | 2.0191 | 74.14% (H-L+4) |
| 10 | 12 | 2.9672 | 417.84 | 2.0206 | 74.63% (H-L+4) |

^a In CI, H is the HOMO and L is the LUMO.

3.5. Reorganization energy, IP, EA and chemical reactivity

The energy required for the reorganization of the molecular structure during charge migration is a key parameter affecting the degree of charge migration, *i.e.*, the reorganization energy. The reorganization energy mainly comes from two parts, one part comes from the difference in the molecular structure before and after charge transfer, which is called internal reorganization energy. The other part comes from the influence of the solvent medium on charge transfer, *i.e.*, the external reorganization energy, but it is difficult to estimate with theoretical accuracy. In our calculations, the changes in internal reorganization energy under different electric fields were calculated, and then the regulation of charge carrier mobility by using the electric field was investigated. In general, the reorganization energy is negatively correlated with the charge mobility, and a smaller reorganization energy is an important factor to ensure good current density. The total internal reorganization energy (λ_{total}) is determined by both electron reorganization energy (λ_e) and hole reorganization energy (λ_h), which can be calculated by using the following equation:^{49,50}

$$\lambda_e = (E_0^- - E_-) + (E_-^0 - E_0) \quad (5)$$

$$\lambda_h = (E_0^+ - E_+) + (E_+^0 - E_0) \quad (6)$$

$$\lambda_{\text{total}} = \lambda_e + \lambda_h \quad (7)$$

$E_0^-(E_0^+)$ is the energy of the anion (cation) based on the optimal ground state geometry, where $E_-(E_+)$ is the energy of the optimal anion (cation) geometry, $E_-^0(E_+^0)$ is the energy of the neutral dye based on the optimal anion (cation) geometry, and E_0 is the energy of the optimal ground state geometry. The reorganization energies of the dye molecule at different F_{ext} are shown in Fig. 7. First, it can be seen from Fig. 7a that when $F_{\text{ext}} = 0$, $\lambda_e = 0.138$ eV and $\lambda_h = 0.262$ eV, λ_h is obviously larger than λ_e , indicating that the electron transfer rate is larger than the hole transfer rate. And in the negative electric field range, except for $F_{\text{ext}} = -10 \times 10^{-5}$ a.u., the λ_e under other electric fields is larger than λ_h , which is opposite to the case of no electric field, indicating that the direction of the electric field does have an impact on the charge transfer. Furthermore, the results show that λ_h tends to decrease as the electric field increases; however, the variation of λ_e with electric field is somewhat different. Compared with the gradual change of λ_h , the large increase of λ_e when $F_{\text{ext}} = -1 \times 10^{-5}$ a.u. indicates that the electron mobility is more sensitive to the direction of the electric field. Compared to 0.8296 eV at $F_{\text{ext}} = -10 \times 10^{-5}$, λ_h at $F_{\text{ext}} = 10 \times 10^{-5}$ a.u. is reduced by 0.39 eV. Comparing the changes of λ_h and λ_e at different electric field strengths shows that, overall, the change of λ_h is larger than that of λ_e . It can be seen that although the variation trends of λ_h and λ_e with the electric field strength are different, when the electric field increases, both have a certain decrease, and λ_{total} also decreases (see Fig. 7b), indicating that the introduction of the forward F_{ext} can indeed promote the charge transfer of the dye.

In addition, the energy barriers for hole and electron injection can be predicted by the ionization potential (IP) and



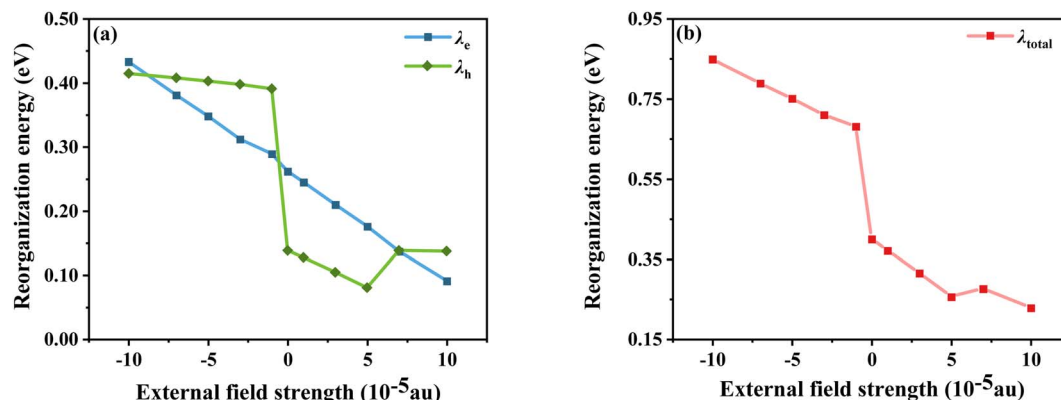


Fig. 7 Electron and hole reorganization energy (a) and total internal reorganization energy (b) in F_{ext} .

electron affinity potential (EA). IP denotes the energy change of absorbed holes (or injected electrons) and EA denotes the energy change of added electrons (or injected holes), which can be expressed as:⁵¹

$$IP = E_0^+ - E_0 \quad (8)$$

$$EA = E_0 - E_0^- \quad (9)$$

In general, a lower IP is favorable to improve ability of hole injection, and a higher EA is favorable to improve the ability of electron injection. As shown in Fig. 8, IP and EA are decreasing and increasing, respectively, with the change in electric field strength. Relative to $IP = 4.884$ eV and $EA = 3.074$ eV at $F_{ext} = -10 \times 10^{-5}$ a.u., IP decreases by about 0.157 eV and EA produces an increment of 0.091 eV at $F_{ext} = 10 \times 10^{-5}$ a.u. From the trends of IP and EA with the F_{ext} , it can be seen that the dye injection ability is continuously improved with the increase in the F_{ext} .

The chemical reaction parameters also affect the optoelectronic properties of DSSCs, so the changes in the chemical reaction parameters of the dye under different electric field strengths were investigated.⁵² Among them, the chemical hardness (h), which is related to the stability and reactivity of the molecular system, describes the resistance to changes in intramolecular charge transfer. As shown in Fig. 9a, the values gradually decrease under the F_{ext} , indicating that its

intramolecular charge transfer characteristics are enhanced with the addition of the F_{ext} . Not only the propensity or ability of a dye to accept electrons can be assessed by measuring the electrophilic index (ω); this index is a measure of the stability of a molecular system after gaining an electron. As shown in Fig. 9b, with the increase of the F_{ext} , ω gradually increases, that is, its energy stability after accepting electrons gradually increases. The electron accepting power (ω^+) evaluated the electron-accepting ability, and the gradually increasing ω^+ under the electric field change indicated the improvement of the electron-attracting ability of the acceptor part, which ensured a good photocurrent efficiency, as seen in Fig. 9c. Thus, in terms of chemical reaction parameters, the dye molecules under the action of a strong electric field exhibit excellent performance.

3.6. Parameters affecting the photovoltaic characteristics of cells

In general, as an important parameter to measure the performance of dyes, PCE (η) can be defined as:⁵³

$$\eta = \frac{J_{sc} V_{oc} FF}{P_{in}} \quad (10)$$

where J_{sc} is the short-circuit current density, V_{oc} is the open-circuit voltage, P_{in} is the incident solar energy on the cell, and FF is the fill factor. The FF can be expressed as the ratio of the

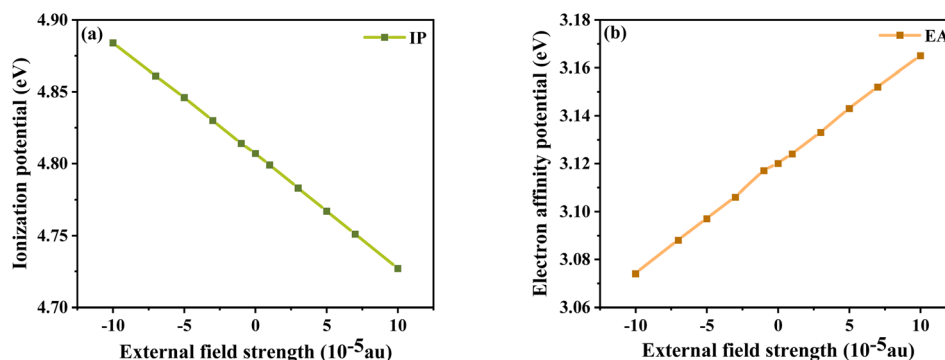


Fig. 8 Ionization potential (a) and electron affinity potential (b) in F_{ext} .



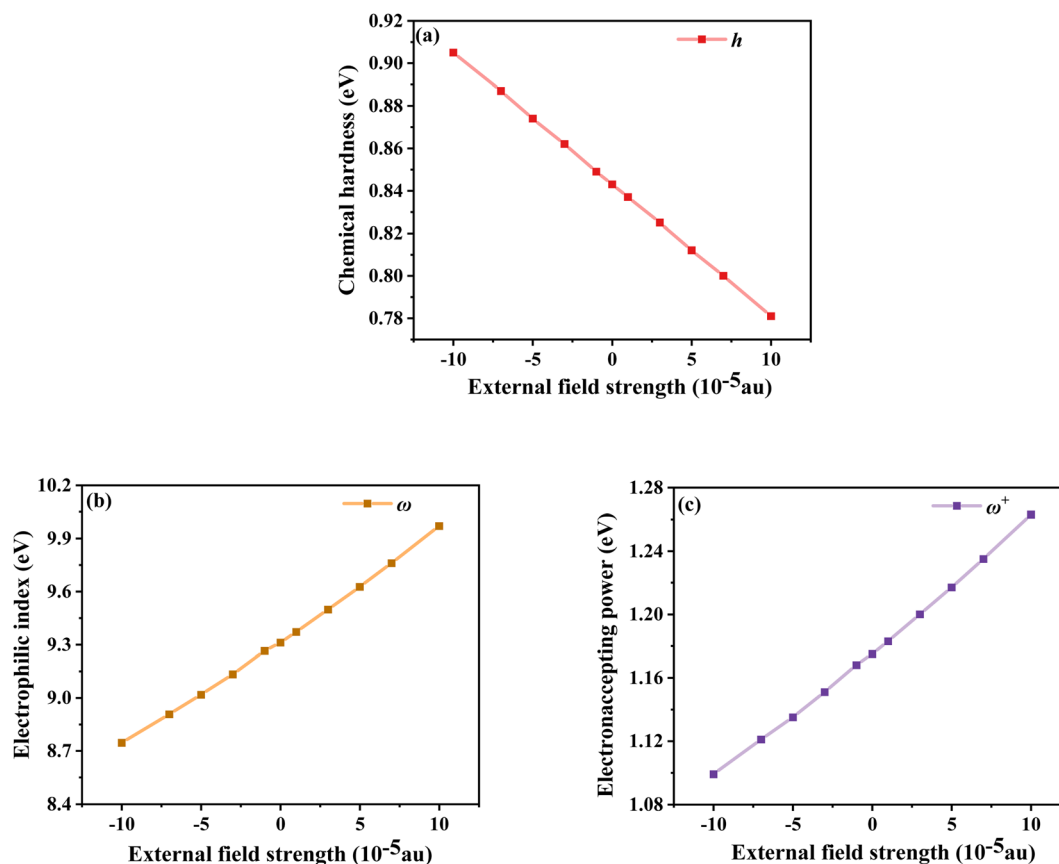


Fig. 9 Chemical hardness (a), electrophilic index (b) and electron accepting power (c) in F_{ext} .

maximum power of the solar cell to the product of J_{sc} and V_{oc} ; however, it is difficult to describe the FF quantitatively because of the complexity of the cell operation process. However, we can characterize the effect of J_{sc} and V_{oc} on the photovoltaic performance of dyes by quantitatively characterizing the parameters that have a major effect on J_{sc} and V_{oc} . J_{sc} in DSSCs can be expressed as:

$$J_{\text{sc}} = \int_{\lambda} \text{LHE}(\lambda) \phi_{\text{inject}} \eta_{\text{collect}} d\lambda \quad (11)$$

where ϕ_{inject} is the electron injection efficiency and η_{collect} is the charge collection efficiency. The same DSSC under different dye conditions has the same η_{collect} , so η_{collect} can be assumed to be a constant. $\text{LHE}(\lambda)$ is the light-harvesting efficiency at the maximum absorption wavelength (λ_{max}), and according to the definition of LHE ($\text{LHE}(\lambda) = 1 - 10^{-f}$), high oscillator strength can ensure better light capture efficiency.^{47,54} To study the effect of F_{ext} on the light response, we calculated the light collection efficiency at the maximum absorption wavelength under different electric fields. The calculated results (Fig. 10) show that the LHE value is close to 1 and the dye molecule has good light trapping ability. Under the action of an electric field, the addition of a negative directional electric field increases the LHE compared to the action of a positive electric field, and the light trapping ability of the dye is the strongest at $F_{\text{ext}} = -10 \times 10^{-5}$ a.u.

On the basis of the efficient light-harvesting ability of dyes, more importantly, the injection of electrons into semiconductors is converted into electric current by means of charge transfer. So enhancing the electron injection efficiency (ϕ_{inject}) of dyes is another way to improve J_{sc} . The ϕ_{inject} is closely associated with the electron injection driving force (ΔG_{inject}), which can be defined as:^{47,54,55}

$$\Delta G_{\text{inject}} = E_{\text{dye}}^* - E_{\text{CB}} = (E_{\text{dye}} - E_{\lambda_{\text{max}}}) - E_{\text{CB}} \quad (12)$$

where E_{dye}^* and E_{dye} are the excited state oxidation potential and ground state redox potential of the dye, respectively, $E_{\lambda_{\text{max}}}$ is the transition energy at λ_{max} , and E_{CB} is the reduction potential at

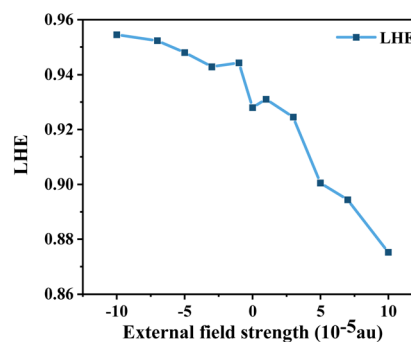


Fig. 10 Light-harvesting efficiency (LHE) in F_{ext} .



the edge of the TiO₂ conduction band, which is usually taken to be −4.0 eV. On the other hand, the ability of dyes to acquire electrons from the electrolyte (dye regeneration) is also a key factor affecting the performance of DSSCs, and the regeneration efficiency can be estimated by quantifying the driving force of regeneration (ΔG_{reg}). According to the redox potential of electrolyte solutions I^-/I_3^- , ΔG_{reg} can be defined as:

$$\Delta G_{\text{reg}} = E_{I^-/I_3^-} - E_{\text{dye}} \quad (13)$$

The calculated E_{dye}^* , E_{dye} , ΔG_{inject} and ΔG_{reg} at different electric fields are shown in Fig. 11. First, it can be found that the calculated ΔG_{inject} is less than zero, and the charge injection process can proceed spontaneously. And the absolute value of ΔG_{inject} is greater than 0.2 eV under all electric field conditions, and the dye molecules have good electron injection efficiency. Moreover, the absolute value of ΔG_{inject} shows an increasing trend when the electric field increases, indicating that the addition of the F_{ext} can further promote the electron injection process of dye molecules. As shown in Fig. 11b, with the change of the F_{ext} , the absolute value of ΔG_{reg} gradually decreases, indicating that the F_{ext} can also improve the regeneration efficiency of the dye. The increase of ΔG_{inject} and the decrease of ΔG_{reg} in general are favorable conditions to ensure a good J_{sc} . Therefore, the addition of the F_{ext} increases the possibility for making dye molecules with higher J_{sc} .

According to eqn (10), the V_{oc} is also an effective factor affecting the cells of dye-sensitized solar energy, which is expressed as:^{56,57}

$$V_{\text{oc}} = \frac{E_{\text{CB}} + \Delta E_{\text{CB}}}{q} + \frac{kT}{q} \ln\left(\frac{n_c}{N_{\text{CB}}}\right) - \frac{E_{\text{redox}}}{q} \quad (14)$$

where E_{CB} is the conduction band edge of the semiconductor, q is the unit charge, kT is the thermal energy at room temperature. n_c and N_{CB} are the number of electrons and the density of states in the conduction band, and E_{redox} is the oxidation potential of the electrolyte. For the same dye molecule, V_{oc} is mainly controlled by the change in the conduction band energy level. The adsorption of dyes can cause charge redistribution, and the change of the electronic structure of TiO₂ will inevitably cause the shift of the E_{CB} (ΔE_{CB}), which in turn affects V_{oc} . Below we discuss how different electric field intensities affect the shift of the E_{CB} induced by dye adsorption, which in turn affects V_{oc} .

Using density functional theory, the total density of states (TDOS) of the dye-TiO₂ system and the partial density of states (PDOS) of the Ti(OH)₃·H₂O monomer were calculated at the B3LYP/6-31G(d) (LANL2DZ for Ti) level.⁵⁸ Smaller clusters may not accurately describe the dye-semiconductor interaction, but our main concern is the relative change of the dye under different electric fields, which should have little effect on the accuracy of the results. Then a linear fit is performed through the low energy range curve (−5 to −3 eV) to obtain the intercept

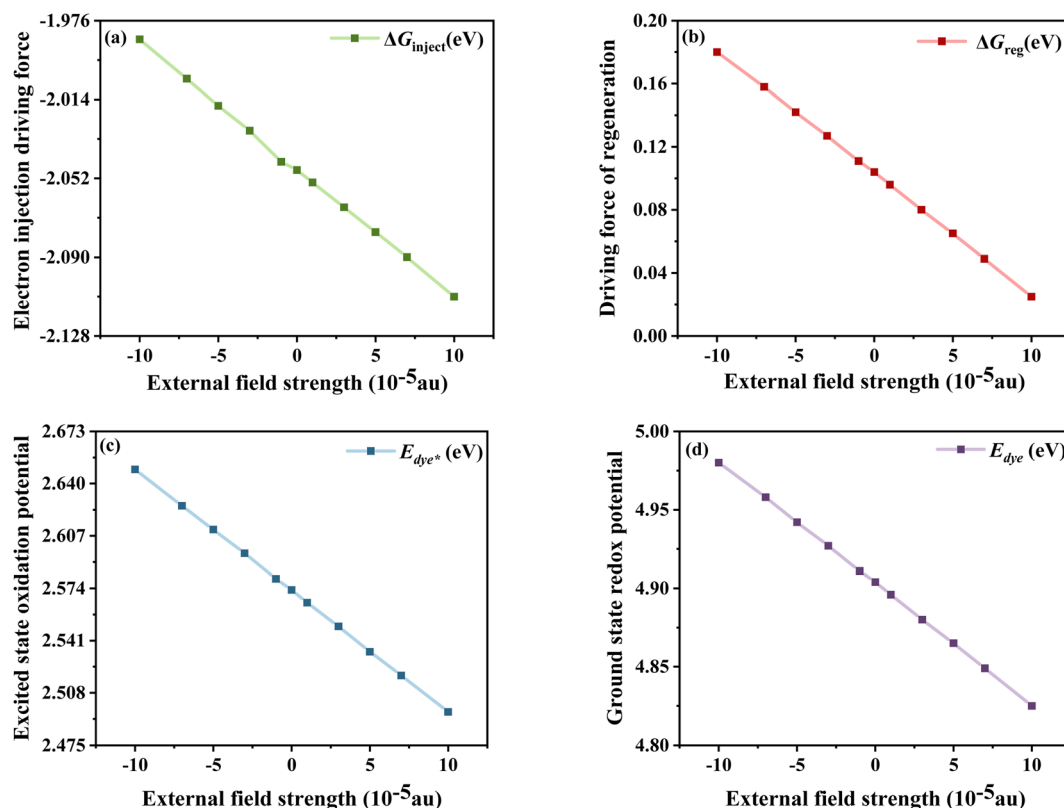


Fig. 11 Electron injection driving force (a), driving force of regeneration (b), excited state oxidation potential of the dye (c) and ground state redox potential of the dye (d) in F_{ext} .



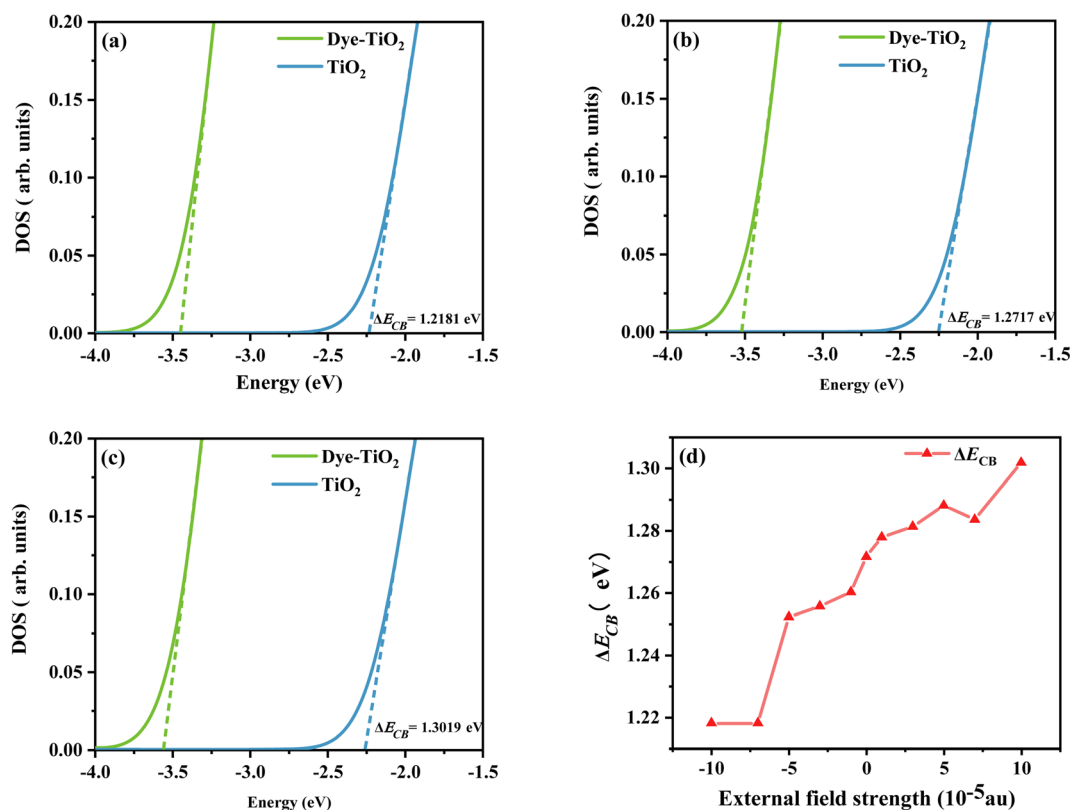


Fig. 12 Schematic diagram of the model to evaluate the ΔE_{CB} due to dye adsorption under the action of $F_{ext} = -10$ (a), $F_{ext} = 0$ (b), and $F_{ext} = 10$ (c), and the variation curve (d) of the ΔE_{CB} in F_{ext} (F_{ext} in 10^{-5} a.u.).

point of the curve with the energy axis. The difference between the intercepts of the TDOS and PDOS lines and the energy axis is ΔE_{CB} (see Fig. 12). As shown in Fig. 12d, the sensitizer adsorption under different F_{ext} can induce the shift of E_{CB} to different degrees. Obviously, ΔE_{CB} generally shows a gradually increasing trend under the change of the F_{ext} . It shows that the dye under the action of strong F_{ext} will show stronger V_{oc} , and then show excellent photovoltaic properties.

4. Conclusion

Using DFT and TD-DFT theories, the photoelectric properties of D-D-A structured dye molecules under the action of the F_{ext} were systematically investigated with the aim of further improving the PCE of DSSCs. We understand the effect of the F_{ext} on the photovoltaic properties of DSSCs by evaluating the key role of relevant parameters affecting PCE. The results show that the dye, under the action of the positive electric field, has better optoelectronic properties than the negative electric field. First, the key photovoltaic properties (ΔG_{inject} , ΔG_{reg} and λ_{total}) under a positive electric field showed significant improvement, indicating that the photocurrent conversion efficiency can be improved to a certain extent. And under the change in electric field strength, the electron affinity ω showed a gradually increasing trend, indicating that the energy stability of the acceptor after accepting electrons gradually increased, ensuring the energy stability of the charge transfer process. Furthermore,

the gradual increase in the change of the conduction band level (ΔE_{CB}) will contribute to better V_{oc} performance. Based on the above discussion, it is hoped that these results of DSSCs under the action of the F_{ext} can provide a theoretical model and provide a valuable reference for the development of more efficient DSSCs in the future.

Conflicts of interest

There are no conflicts to declare.

Acknowledgements

This work was supported by the National Natural Science Foundation of China (Grant No. 11974152), the Science program of the Liaoning Provincial Department of Education (LJKZ0097), and the intercollegiate cooperation project of colleges and universities of Liaoning Provincial Department of Education.

References

- Q. Huahmél, V. M. Mwalukuku, D. Joly, J. Liotier, Y. Kervella, P. Maldivi, S. Narbey, F. Oswald, A. J. Riquelme, J. A. Anta and R. Demadrille, *Nat. Energy*, 2020, 5, 468–477.
- J.-M. Ji, H. Zhou, Y. K. Eom, C. H. Kim and H. K. Kim, *Adv. Energy Mater.*, 2020, 10, 2000124.



- 3 D. Zhang, M. Stojanovic, Y. Ren, Y. Cao, F. T. Eickemeyer, E. Socie, N. Vlachopoulos, J.-E. Moser, S. M. Zakeeruddin, A. Hagfeldt and M. Grätzel, *Nat. Commun.*, 2021, **12**, 1777.
- 4 K. Kakiage, Y. Aoyama, T. Yano, K. Oya, J.-i. Fujisawa and M. Hanaya, *Chem. Commun.*, 2015, **51**, 15894–15897.
- 5 Z. Yao, H. Wu, Y. Li, J. Wang, J. Zhang, M. Zhang, Y. Guo and P. Wang, *Energy Environ. Sci.*, 2015, **8**, 3192–3197.
- 6 M. A. Green, K. Emery, Y. Hishikawa, W. Warta and E. D. Dunlop, *Prog. Photovoltaics*, 2016, **24**, 3–11.
- 7 F. A. Black, C. J. Wood, S. Ngwerume, G. H. Summers, I. P. Clark, M. Towrie, J. E. Camp and E. A. Gibson, *Faraday Discuss.*, 2017, **198**, 449–461.
- 8 M. K. Brennaman, R. J. Dillon, L. Alibabaei, M. K. Gish, C. J. Dares, D. L. Ashford, R. L. House, G. J. Meyer, J. M. Papanikolas and T. J. Meyer, *J. Am. Chem. Soc.*, 2016, **138**, 13085–13102.
- 9 Y. Li, X. Li and Y. Xu, *Spectrochim. Acta, Part A*, 2020, **234**, 118241.
- 10 Y. Hao, W. Yang, L. Zhang, R. Jiang, E. Mijangos, Y. Saygili, L. Hammarström, A. Hagfeldt and G. Boschloo, *Nat. Commun.*, 2016, **7**, 13934.
- 11 K. Cai, H. Wu, T. Hua, C. Liao, H. Tang, L. Wang and D. Cao, *Dyes Pigm.*, 2022, **197**, 109922.
- 12 M. Hosseinneshad, S. Nasiri, M. Fathi, M. Ghahari and K. Gharanjig, *Opt. Mater.*, 2022, **124**, 111999.
- 13 P. S. Gangadhar, A. Jagadeesh, M. N. Rajesh, A. S. George, S. Prasanthkumar, S. Soman and L. Giribabu, *Adv. Mater.*, 2022, **3**, 1231–1239.
- 14 L. Jin, S. Shi, C. Zhao, X. Yu, J. Lu, Q. Wang and Y. Wei, *J. Power Sources*, 2021, **481**, 228952.
- 15 A. K. Singh, A. N. Veetil and J. Nithyanandhan, *ACS Appl. Energy Mater.*, 2021, **4**, 3182–3193.
- 16 M. Miyashita, K. Sunahara, T. Nishikawa, Y. Uemura, N. Koumura, K. Hara, A. Mori, T. Abe, E. Suzuki and S. Mori, *J. Am. Chem. Soc.*, 2008, **130**, 17874–17881.
- 17 A. Mishra, M. K. Fischer and P. Bäuerle, *Angew. Chem., Int. Ed. Engl.*, 2009, **48**, 2474–2499.
- 18 L. Han, J. Liu, Y. Liu and Y. Cui, *J. Mol. Struct.*, 2019, **1180**, 651–658.
- 19 T. G. Deepak, G. S. Anjusree, S. Thomas, T. A. Arun, S. V. Nair and A. Sreekumaran Nair, *RSC Adv.*, 2014, **4**, 17615–17638.
- 20 H. Li, Y. Hou, Y. Yang, R. Tang, J. Chen, H. Wang, H. Han, T. Peng, Q. Li and Z. Li, *ACS Appl. Mater. Interfaces*, 2013, **5**, 12469–12477.
- 21 S. Kotteswaran and P. Ramasamy, *New J. Chem.*, 2021, **45**, 2453–2462.
- 22 G. R. Kandregula, S. Mandal, G. Prince, S. K. Yadav and K. Ramanujam, *New J. Chem.*, 2020, **44**, 4877–4886.
- 23 L. Jean-Gérard, W. Vasseur, F. Scherninski and B. Andrioletti, *Chem. Commun.*, 2018, **54**, 12914–12929.
- 24 R. S. Rao, B. Yadagiri, G. D. Sharma and S. P. Singh, *Chem. Commun.*, 2019, **55**, 12535–12538.
- 25 G. D. Sharma, S. A. Siddiqui, A. Nikiforou, G. E. Zervaki, I. Georgakaki, K. Ladomenou and A. G. Coutsolelos, *J. Mater. Chem. C*, 2015, **3**, 6209–6217.
- 26 A. Benitz, M. B. Thomas, Y. Jang, V. Nesterov and F. D'Souza, *J. Chem. Sci.*, 2021, **133**, 71.
- 27 P. Besalu-Sala, A. A. Voityuk, J. M. Luis and M. Sola, *Phys. Chem. Chem. Phys.*, 2021, **23**, 5376–5384.
- 28 S. Mukherjee, F. Libisch, N. Large, O. Neumann, L. V. Brown, J. Cheng, J. B. Lassiter, E. A. Carter, P. Nordlander and N. J. Halas, *Nano Lett.*, 2013, **13**, 240–247.
- 29 X. Lu, Y. Sun and W. Hu, *J. Mater. Chem. A*, 2021, **9**, 21044–21050.
- 30 P. Song, Y. Li, F. Ma and M. Sun, *J. Mater. Chem. C*, 2015, **3**, 4810–4819.
- 31 P. Song, Y. Li, F. Ma, T. Pullerits and M. Sun, *J. Phys. Chem. C*, 2013, **117**, 15879–15889.
- 32 M. J. Frisch, G. W. Trucks, H. B. Schlegel, G. E. Scuseria, M. A. Robb, J. R. Cheeseman, G. Scalmani, V. Barone, G. A. Petersson, H. Nakatsuji, X. Li, M. Caricato, A. V. Marenich, J. Bloino, B. G. Janesko, R. Gomperts, B. Mennucci, H. P. Hratchian, J. V. Ortiz, A. F. Izmaylov, J. L. Sonnenberg, D. Williams-Young, F. Ding, F. Lipparini, F. Egidi, J. Goings, B. Peng, A. Petrone, T. Henderson, D. Ranasinghe, V. G. Zakrzewski, J. Gao, N. Rega, G. Zheng, W. Liang, M. Hada, M. Ehara, K. Toyota, R. Fukuda, J. Hasegawa, M. Ishida, T. Nakajima, Y. Honda, O. Kitao, H. Nakai, T. Vreven, K. Throssell, J. A. Montgomery Jr, J. E. Peralta, F. Ogliaro, M. J. Bearpark, J. J. Heyd, E. N. Brothers, K. N. Kudin, V. N. Staroverov, T. A. Keith, R. Kobayashi, J. Normand, K. Raghavachari, A. P. Rendell, J. C. Burant, S. S. Iyengar, J. Tomasi, M. Cossi, J. M. Millam, M. Klene, C. Adamo, R. Cammi, J. W. Ochterski, R. L. Martin, K. Morokuma, O. Farkas, J. B. Foresman and D. J. Fox, *Gaussian 09*, Gaussian, Inc., Wallingford CT, 2016.
- 33 P. Hohenberg and W. Kohn, *Phys. Rev.*, 1964, **136**, B864–B871.
- 34 E. K. Gross and W. Kohn, *Phys. Rev. Lett.*, 1985, **55**, 2850–2852.
- 35 A. D. Becke, *Phys. Rev. A*, 1988, **38**, 3098–3100.
- 36 V. A. Rassolov, M. A. Ratner, J. A. Pople, P. C. Redfern and L. A. Curtiss, *J. Comput. Chem.*, 2001, **22**, 976–984.
- 37 J. D. Dill and J. A. Pople, *J. Chem. Phys.*, 1975, **62**, 2921–2923.
- 38 M. M. Francel, W. J. Pietro, W. J. Hehre, J. S. Binkley, M. S. Gordon, D. J. DeFrees and J. A. Pople, *J. Chem. Phys.*, 1982, **77**, 3654–3665.
- 39 P. J. Hay and W. R. Wadt, *J. Chem. Phys.*, 1985, **82**, 299–310.
- 40 A. D. Becke, *J. Chem. Phys.*, 1993, **98**, 1372–1377.
- 41 T. Lu and F. Chen, *J. Comput. Chem.*, 2012, **33**, 580–592.
- 42 T. Yanai, D. P. Tew and N. C. Handy, *Chem. Phys. Lett.*, 2004, **393**, 51–57.
- 43 M. Cossi and V. Barone, *J. Chem. Phys.*, 2001, **115**, 4708–4717.
- 44 C. Adamo and V. Barone, *Chem. Phys. Lett.*, 2000, **330**, 152–160.
- 45 F. Sim, S. Chin, M. Dupuis and J. E. Rice, *J. Phys. Chem. C*, 1993, **97**, 1158–1163.
- 46 K. B. Sophy, P. Calaminici and S. Pal, *J. Chem. Theory Comput.*, 2007, **3**, 716–727.
- 47 M. K. Nazeeruddin, R. Humphry-Baker, P. Liska and M. Grätzel, *J. Phys. Chem. B*, 2003, **107**, 8981–8987.
- 48 R. Sánchez-de-Argas, M. Á. San Miguel, J. Oviedo and J. F. Sanz, *Phys. Chem. Chem. Phys.*, 2012, **14**, 225–233.



- 49 A. Fitri, A. T. Benjelloun, M. Benzakour, M. McHarfi, M. Hamidi and M. Bouachrine, *Spectrochim. Acta, Part A*, 2014, **124**, 646–654.
- 50 M. P. Balanay and D. H. Kim, *J. Mol. Struct. THEOCHEM*, 2009, **910**, 20–26.
- 51 Z.-L. Zhang, L.-Y. Zou, A.-M. Ren, Y.-F. Liu, J.-K. Feng and C.-C. Sun, *Dyes Pigm.*, 2013, **96**, 349–363.
- 52 Y. Li, X. Li and Y. Xu, *Spectrochim. Acta, Part A*, 2020, **234**, 118241.
- 53 M. R. Narayan, *Renewable Sustainable Energy Rev.*, 2012, **16**, 208–215.
- 54 F. Arkan, M. Izadyar and A. Nakhaeipour, *Energy*, 2016, **114**, 559–567.
- 55 W. Sang-aaron, S. Saekow and V. Amornkitbamrung, *J. Photochem. Photobiol., A*, 2012, **236**, 35–40.
- 56 T. Marinado, K. Nonomura, J. Nissfolk, M. K. Karlsson, D. P. Hagberg, L. Sun, S. Mori and A. Hagfeldt, *Langmuir*, 2010, **26**, 2592–2598.
- 57 S.-B. Li, D.-M. Gu, J. Zhang, Y. Geng, M. Zhang and Z.-M. Su, *New J. Chem.*, 2016, **40**, 9320–9328.
- 58 E. Ronca, M. Pastore, L. Belpassi, F. Tarantelli and F. De Angelis, *Energy Environ. Sci.*, 2013, **6**, 183–193.

